Journal of Magnetic Resonance 210 (2011) 126–132

Contents lists available at ScienceDirect

Journal of Magnetic Resonance

journal homepage: www.elsevier.com/locate/jmr

Continuous-wave EPR at 275 GHz: Application to high-spin Fe^{3+} systems

G. Mathies [a,*], H. Blok [a], J.A.J.M. Disselhorst [a], P. Gast [a], H. van der Meer [a], D.M. Miedema [a], R.M. Almeida [b], J.J.G. Moura [b], W.R. Hagen [c], E.J.J. Groenen [a,*]

[a] Department of Molecular Physics, Huygens Laboratory, Leiden University, The Netherlands
[b] Department of Chemistry, Universidade Nova de Lisboa, Portugal
[c] Department of Biotechnology, Delft University of Technology, The Netherlands

ARTICLE INFO

Article history:
Received 23 November 2010
Revised 2 March 2011
Available online 11 March 2011

Keywords:
EPR
High-field
High-frequency
Continuous-wave
Single-mode cavity
Fe(III)–EDTA
Rubredoxin

ABSTRACT

The 275 GHz electron-paramagnetic-resonance spectrometer we reported on in 2004 has been equipped with a new probe head, which contains a cavity especially designed for operation in continuous-wave mode. The sensitivity and signal stability that is achieved with this new probe head is illustrated with 275 GHz continuous-wave spectra of a 1 mM frozen solution of the complex Fe(III)-ethylenediamine tetra-acetic acid and of 10 mM frozen solutions of the protein rubredoxin, which contains Fe^{3+} in its active site, from three different organisms. The high quality of the spectra of the rubredoxins allows the determination of the zero-field-splitting parameters with an accuracy of 0.5 GHz. The success of our approach results partially from the enhanced absolute sensitivity, which can be reached using a single-mode cavity. At least as important is the signal stability that we were able to achieve with the new probe head.

1. Introduction

The understanding of complex electron-paramagnetic-resonance (EPR) spectra of the active sites of metalloproteins is often greatly advanced by studies at more than one microwave frequency. High-frequency/high-field (HF) EPR is particularly useful for systems that have a large zero-field splitting. Integer spin systems tend to be EPR silent at conventional microwave frequencies and for half-integer spin systems the ease and precision by which the zero-field-splitting parameters can be determined is enhanced. The goal of this work is to extend the possibilities of HF EPR for metalloproteins.

The HF EPR spectra of metalloproteins with a zero-field splitting on the order of the microwave quantum are difficult to record. These spectra cover large field ranges. Due to conformational strain the resonances in the HF EPR spectra are broad, and line widths of 1 T are no exception. Moreover, the available amount of protein is often limited and the same holds for the concentration. Relaxation times can be very short, which makes only continuous-wave (cw) EPR feasible. In order to achieve our goal, we need a HF cw EPR spectrometer with high sensitivity and signal stability, which is maintained while using a large modulation amplitude.

High-frequency/high-field EPR was introduced by the group of Lebedev in Moscow [1–3]. Their spectrometer operated at a frequency of 140 GHz, which is the highest frequency at which conventional waveguides can be used. Indeed, HF EPR comes with technical difficulties. Major progress was made by the introduction of quasi-optical techniques and in the development of high-frequency microwave components and high-field magnets. Spectrometers that operate in cw mode at frequencies above 140 GHz are found in specialized research groups at Cornell (250 GHz [4] and 100–300 GHz [5]), in Grenoble (160–525 GHz [6–8]), St. Andrews (80–200 GHz [9]), Berlin (360 GHz [10]), Tallahassee (24 GHz–3 THz [11,12]), Frankfurt (180 GHz [13]), Leiden (275 GHz [14,15]) and Mülheim an der Ruhr (244 GHz [16]). This year Bruker has released a spectrometer that operates at 263 GHz.[1] For recent reviews see Refs. [17,18].

In 2004 we reported on the construction of a cw and pulsed EPR spectrometer operating at 275 GHz [14]. This spectrometer is equipped with a multi-functional TE_{011} cylindrical cavity, which has slits to allow optical access and electron nuclear double resonance [15]. With this cavity it is possible to measure cw EPR of paramagnetic species that have narrow resonances (for instance spin-labels), but spectra of species that show broad resonances are poor. Our approach to improve the quality of these spectra is to equip the spectrometer with a second probe head, which contains a single-mode cavity optimized for operation in cw mode.

* Corresponding authors.
E-mail addresses: mathies@physics.leidenuniv.nl (G. Mathies), groenen@physics.leidenuniv.nl (E.J.J. Groenen).

[1] http://www.bruker-biospin.com/e780.html.

1090-7807/$ - see front matter © 2011 Elsevier Inc. All rights reserved.
doi:10.1016/j.jmr.2011.03.009

Currently all other HF cw EPR spectrometers operate in non-resonant transmission or reflection or use a Fabry–Perot interferometer. However the use of a single-mode cavity has several advantages. First, one can profit from the increase of the absolute sensitivity with an increasing microwave frequency, which theory predicts [19–22]. Secondly, the high B_1-field at the sample, which can be generated with a single-mode cavity, is advantageous for fast-relaxing species. Finally, the small sample volume makes it relatively easy to achieve a high, homogeneous modulation field throughout the sample. Drawbacks of using a single-mode cavity could be sample handling and the problem of constructing a single-mode cavity of the dimensions that fit 275 GHz, but the former is not a problem for solutions of proteins due to the capillary force and we already showed that we could overcome the latter.

An ever persisting problem in cw HF EPR is signal stability. The high magnetic field induces strong Lorentz forces on the modulation coil, which cause vibrations in the probe head at the modulation frequency or its harmonics. This is called microphonics [9,23,24]. This interference tends to be in phase with the modulated EPR signal and can seriously deteriorate the signal-to-noise ratio. This is particularly a problem when recording broad resonances with a large modulation amplitude. Operation in induction mode can reduce the effect of microphonics on the EPR signal [9,25], but this is not an option when a single-mode cavity is used. We show that the use of a single-mode cavity also allows the reduction of the influence of microphonics such that high-quality spectra of frozen solutions of low concentrations of metalloproteins can be recorded.

The achieved sensitivity and stability is illustrated by 275 GHz cw EPR spectra of a 1 mM frozen solution of the complex Fe(III)-ethylenediamine tetra-acetic acid (EDTA) and of 10 mM frozen solutions of the protein rubredoxin, which contains Fe^{3+} in its active site. The iron ion is in a high-spin state, which leaves five unpaired electrons ($S = 5/2$). We have chosen Fe(III)–EDTA as a model complex to demonstrate the performance of our spectrometer, because of its representative spectrum and because several HF EPR studies have been performed on frozen solutions of Fe(III)–EDTA on other spectrometers [16,26–28]. Rubredoxins are small proteins (typically 50–54 amino acids) that are found in sulfur-metabolizing bacteria and archaea, in which they participate in single-electron transfer. They have been studied extensively [29]. The iron ion in the active site is approximately tetrahedrally coordinated to the sulfur atoms of four cysteine residues occurring in a Cys-x-x-Cys-Gly and a Cys-Pro-x-Cys-Gly segment. Our studies show that we are able to acquire high-quality HF cw EPR spectra of small amounts of dilute frozen solutions of high-spin Fe^{3+} systems.

2. Experimental

2.1. The cw probe head

The cw probe head is similar to the probe head that contained the general purpose cavity [14]. This probe head can be placed into a helium flow cryostat located in the room temperature bore of the superconducting magnet. The microwaves are guided through an oversized corrugated waveguide, which ends in a corrugated tapered transition to a fundamental-mode rectangular waveguide from where the microwaves couple into the cavity.

Fig. 1 shows a drawing of the cavity. The design considerations for the cw cavity were to have a high quality factor and to minimize microwave leakage, since this could destabilize the EPR signal. The cavity is a 14 mm long cylinder with a diameter of 1.40 mm in a massive bronze block, which was made by electrical discharge machining. It was polished with diamond paste and gold plated. At both open ends of the cylinder a bronze plunger enters,

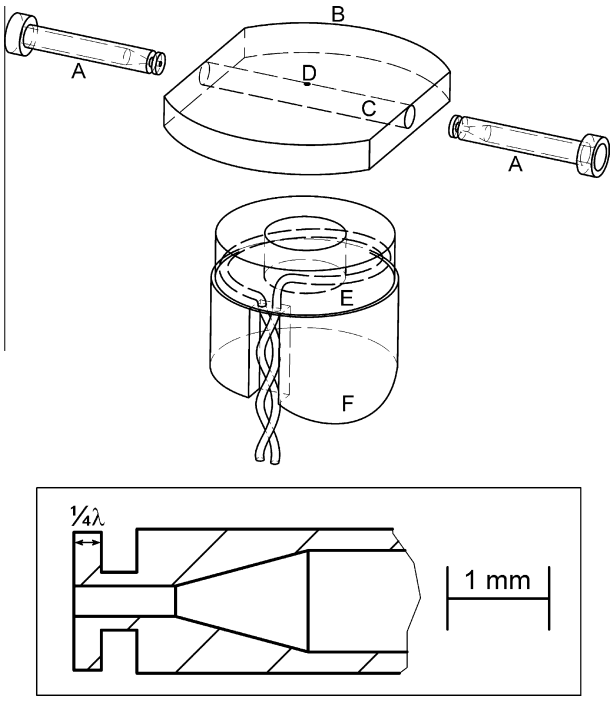

Fig. 1. Schematic drawing of the 275 GHz cw cavity and the modulation coil. A: plungers, B: cavity block, C: cavity, D: coupling hole, E: modulation coil encased in Stycast (for clarity only one turn is depicted) F: modulation coil mount. The inset shows the choke joint at the end of the plungers in detail.

which has a choke joint at the front. We tune the cavity to the microwave frequency of 275.7 GHz by moving the plungers in or out of the cylinder using a set of gears. The length of the cavity can be varied in this way between 0.80 and 1.40 mm with a position accuracy of 1 μm. A quartz sample tube with outer diameter 0.25 mm can be inserted into the cavity through the plungers. With an inner diameter of 0.15 mm the sample volume inside the cavity is 25 nl. The coupling between the fundamental-mode rectangular waveguide and the cavity is varied by rotating the cavity-plunger-gear combination around a vertical axis through the rectangular waveguide and the coupling hole.

Also shown in Fig. 1 is the modulation coil. The modulation coil consists of 80 turns of 0.2 mm diameter copper wire, which are encased in Stycast epoxy. The coil is placed on a solid rexolite mount, which is fixed on a pertinax plate, which is attached to the end of the probe head. The distance between the coil and the cavity block is 0.5 mm, and the two are mechanically isolated. The modulation coil leads are fixed to the mount with Stycast and go up to the top of the probe head as a twisted pair. The resistance of the modulation coil at room temperature is about 1 Ω. The modulation amplitude is 7 mT/A peak-peak.

2.2. Samples

Fe(III)–EDTA sodium salt (Sigma–Aldrich Chemie GmbH) was dissolved in an aqueous solution which was kept at pH 5 by a citric acid buffer. Samples consisted of one part of this solution and one part glycerol. Rubredoxin from *Desulfovibrio gigas* [30,31] was purified according to a previously reported method [32]. To ensure that no other metal forms of rubredoxin, other than iron, were present in the sample, the protein was injected in a 6 ml Resource Q column (GE Biosciences) equilibrated with 10 mM Tris–HCl pH 7.6 buffer and eluted in a linear NaCl gradient (0–500 mM in buffer). Throughout the purification procedure the purity of the rubredoxin fractions was assessed by SDS-PAGE, and by measuring the

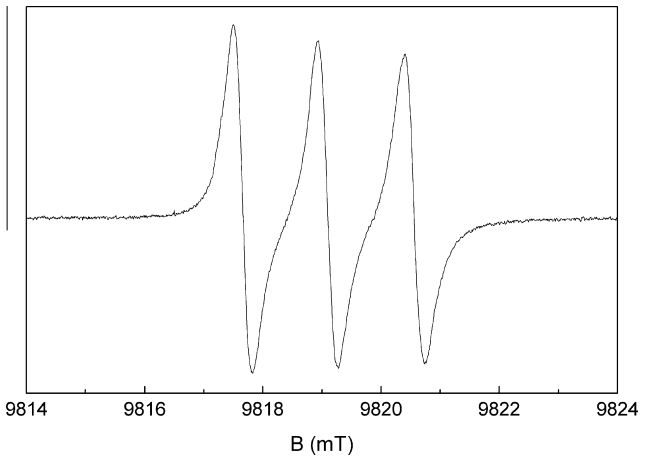

Fig. 2. The room temperature cw EPR spectrum at 275 GHz of a 10^{-4} M solution of the spin label TEMPO in toluene. Experimental conditions: modulation amplitude: 0.05 mT, time constant: 100 ms, microwave power: 50 μW.

A_{280}/A_{493} ratio, which for pure Fe-rubredoxin is 2.4. Rubredoxin from *Pyrococcus furiosus* [33,34] and *Megasphaera elsdenii* were prepared as described in Refs. [35,36] respectively.

3. Results

3.1. Absolute sensitivity

In Fig. 2 the room temperature 275 GHz cw EPR spectrum of a 10^{-4} M solution of the spin label TEMPO (Sigma–Aldrich Chemie GmbH) in toluene is shown. This spectrum was recorded using a modulation amplitude of 0.05 mT, a time constant of 100 ms and a microwave power of 50 μW.[2] The three lines originate from the hyperfine interaction with the ^{14}N nuclear spin ($I = 1$). We determine the absolute sensitivity of our spectrometer from this spectrum. Assuming that the volume of the sample that contributes to the EPR signal is one-third of the sample volume inside the cavity, the spectrum originates from 10^{12} spins. The signal-to-noise ratio of the spectrum shown in Fig. 2 is 320. The total line width of the spectrum is 3×0.35 mT = 1.05 mT. This gives an absolute sensitivity of 8×10^8 spins/mT/$\sqrt{Hz}$.

3.2. Operating the spectrometer in cw mode

Microphonics are observed as an unstable component at the modulation frequency in the frequency spectrum of the output voltage of the detection diode. This component, which is not related to absorption of microwaves by the paramagnetic sample, becomes stronger as the magnetic field strength is increased. Tuning the cavity by moving the plungers with care brings down this modulation frequency pick-up. If the cavity is properly tuned the reflection of the microwaves by the cavity is at a minimum, which means that a small detuning of the cavity will hardly affect the reflection. It is thus necessary to tune at a high magnetic-field strength where no EPR signal is observed.

The high-spin Fe^{3+} spectra are recorded with a scan rate of 2 mT/s and acquiring these spectra takes hours. The microwave frequency of the current bridge of our spectrometer is fixed. This means that we have to take care to keep conditions inside the cryostat constant. Small variations in temperature and helium pressure inside the flow cryostat may detune the cavity, which leads to drift of the baseline of the EPR spectrum and increases the effect that microphonics have on the EPR signal. The use of a high modulation amplitude is essential to detect the broad resonances of Fe^{3+}. This makes minimization of microphonics even more challenging. In practice a modulation current of about 600 mA was found to be optimal. No dependence of the microphonics on the modulation frequency was found. The modulation frequency was chosen between 1 and 2 kHz.

A decrease of the sample temperature does not automatically mean an increase of the sensitivity of the spectrometer. When the probe head is cooled by cold helium gas, the circumstances in the cavity, which have a strong influence on the reflected microwaves, tend to vary more strongly. This has a negative effect on the signal stability. Also the quality factor of the cavity increases strongly as it is cooled down, due to an increase in the conductivity of the gold-plated walls of the cavity. An increased quality factor means an increase in the effect on the EPR signal of a slight detuning of the cavity which means that microphonics become more of a problem. In order to compensate for this effect we had to attenuate the microwave power in order to record the Fe^{3+} spectra.

3.3. High-spin Fe^{3+} spectra

In Fig. 3 the cw EPR spectra recorded at 275 GHz of a 1 mM frozen solution of Fe(III)–EDTA are shown. The recorded spectra cover 6 T. Around 6.6 T a resonance with a width of 0.5 T is observed. As the temperature is increased, this resonance decreases in intensity, while the resonances in the $g = 2$ region gain intensity ($g = 2$ corresponds to a magnetic field of 9.85 T for 275.7 GHz). In Fig. 4 the $g = 2$ region is shown in detail. The signal-to-noise ratio for the

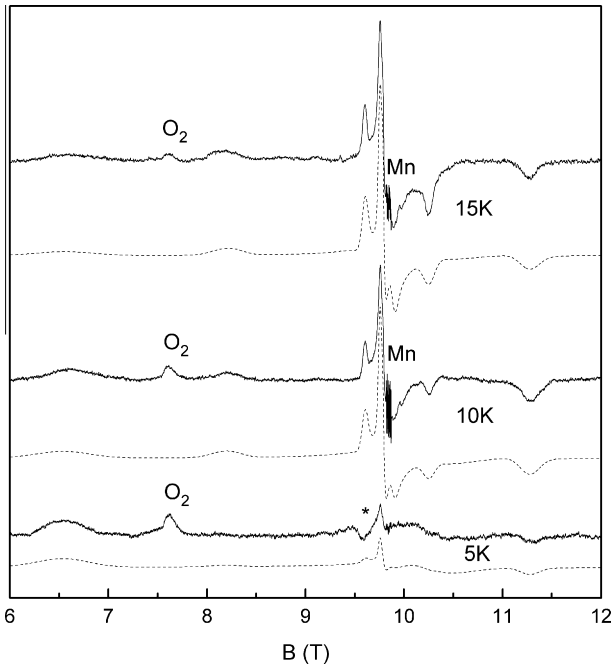

Fig. 3. The 275 GHz cw EPR spectra of a 1 mM frozen solution of the model complex Fe(III)–EDTA at three temperatures. Experimental conditions: modulation amplitude: 3 mT, time constant: 1 s, scan rate: 2 mT/s, microwave power: 1 μW. Spectra were recorded at least twice to ensure reproducibility of all features. The solid lines are the experimentally observed spectra and the dashed lines are the spectra calculated by EasySpin with the parameters given in Table 1. The origin of the resonance marked with a ★ in the 5 K spectrum is unknown. In the 10 K spectrum a weak EPR signal between 8.5 and 9.5 T that does not originate from the Fe(III)–EDTA was subtracted for clarity.

[2] The power output of the microwave bridge is 1 mW, but the maximum power that can be used in cw experiments at room temperature is about 50 μW. Coupling of the microwaves into the cavity is not fully critical and at higher output powers reflected microwaves cause saturation in the detection path.

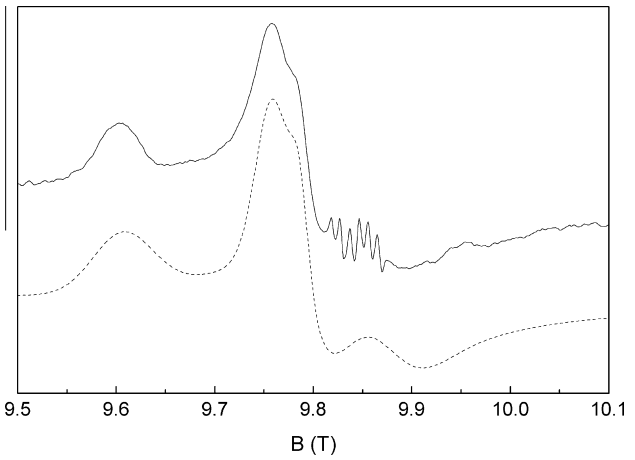

Fig. 4. Detail of the 275 GHz cw EPR spectrum of a 1 mM frozen solution of the model complex Fe(III)–EDTA at 15 K in Fig. 3. The solid line is the experimentally observed spectrum and the dashed line is the spectrum calculated by EasySpin with the parameters given in Table 1.

resonance around 9.8 T (peak to peak) at 15 K is 130. Another resonance is observed around 8.2 T, which is equidistant with the resonances around 6.6 T and 9.8 T. Two more resonances are observed around 10.2 T and 11.3 T. Note that the resonances are broadest at the extremes of the spectrum. Resonances which do not originate from Fe(III)–EDTA are distinguishable in the spectra. At temperatures above 5 K in the $g = 2$ region six lines due to a manganese impurity could be properly recorded by scanning slowly with a lower modulation amplitude. The resonance at 7.6 T is due to a contamination of the frozen sample solution with molecular oxygen [37]. The origin of the resonance that is observed at 9.6 T in the 5 K spectrum is not known.

Fig. 5 shows cw EPR spectra recorded at 275 GHz of a frozen solution of the protein rubredoxin from *D. gigas*. The recorded spectra cover 12 T and resonances of a width of 1 T are observed. The resonances that are observed at low field (up to 4 T) lose intensity with temperature. Broad resonances around 6.8 T, 8.7 T, 10.2 T and 11.3 T increase in intensity upon an increase in temperature from 5 to 10 K. In the $g = 2$ region resonances at 9.5 T and 9.7 T appear at higher temperature. The signal-to-noise ratio for the resonance at 9.7 T (peak to peak) at 25 K is 200. At 4.4 T and 7.6 T resonances due to molecular oxygen are seen [37]. As in the Fe(III)–EDTA spectra, a resonance of unknown origin is observed at 9.6 T in the 5 K spectrum. The narrow resonance at 9.8 T ($g \approx 2$) that is visible at 10 and 25 K is due to an impurity.

In Fig. 6 cw EPR spectra recorded at 275 GHz of rubredoxin from three different species are compared. The spectra are similar, but the precise position of the resonances around 6.8 T, 8.7 T, 10.2 T and 11.3 T varies for the different species by a few tens of mT. Also the shape of the spectra of rubredoxin from *P. furiosus* and in particular from *M. elsdenii* differs from that of the spectrum from *D. gigas*. For these two species of rubredoxin a broad background signal seems to be present. A manganese resonance is observed in the spectrum of rubredoxin from *P. furiosus*.

4. Analysis

The following spin Hamiltonian was used to analyze the spectra of high-spin Fe^{3+}($S = 5/2$).

$$\widehat{H} = \mu_B \widetilde{\mathbf{S}}\mathbf{g}\mathbf{B} + \widetilde{\mathbf{S}}\mathbf{D}\mathbf{S} \tag{1}$$

A tilde is used to represent a transposed vector. The first term is the electron Zeeman term. A first-order contribution from spin-orbit

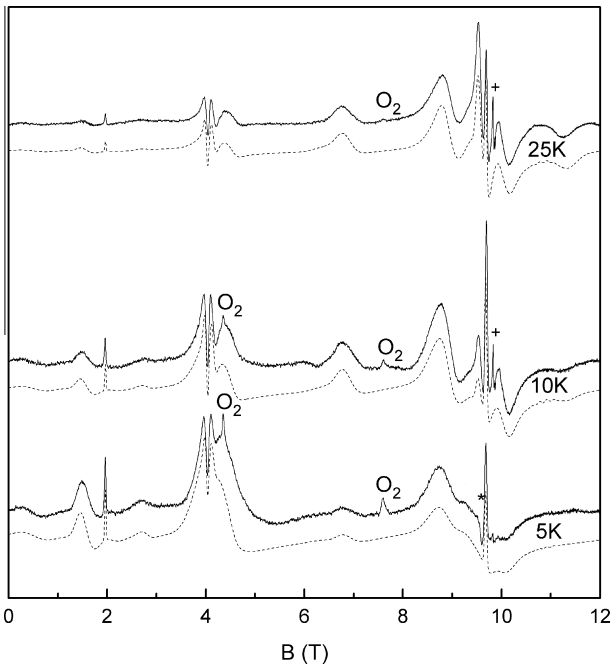

Fig. 5. The 275 GHz cw EPR spectra of a 10 mM frozen solution of the protein rubredoxin from *D. gigas* at three temperatures. Experimental conditions: modulation amplitude: 4 mT, time constant: 1 s, scan rate: 2 mT/s, microwave power: 1 μW. The solid lines are the experimentally observed spectra and the dashed lines are the spectra calculated by EasySpin with the parameters given in Table 1. The origin of the resonance marked with a ☆ in the 5 K spectrum is unknown. The resonance marked with a + in the 10 K and 25 K spectra derives from an impurity.

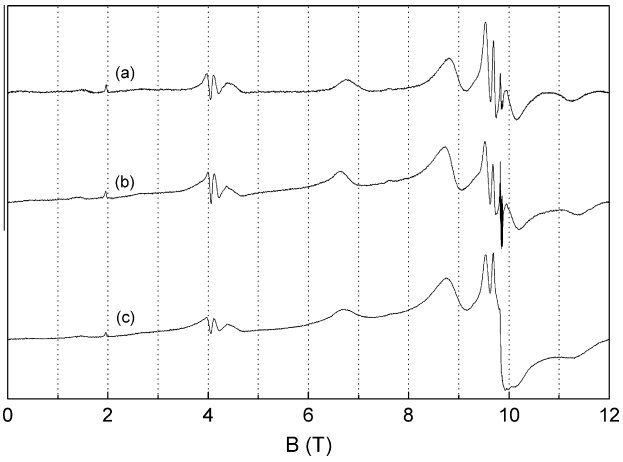

Fig. 6. The cw EPR spectra of 10 mM frozen solutions of rubredoxin from three different organisms at 25 K: (a) *D. gigas*, (b) *P. furiosus*, and (c) *M. elsdenii*. The vertical dashed lines are displayed to guide the eye to the differences between the three spectra. Simulations of the spectra of rubredoxin from *P. furiosus* and *M. elsdenii* are presented in Supplementary Material.

coupling induces *g*-anisotropy, but this effect is expected to be small, since high-spin Fe^{3+} has a $^6S_{5/2}$ ground state. The second term is a field independent fine-structure term (the zero-field splitting, ZFS). The tensor **D** mainly consists of a second-order contribution from spin-orbit coupling. It is symmetric and taken traceless, and it can be characterized by two parameters, *D* and *E*.

$$D = \frac{3}{2}D_z, \quad E = \frac{1}{2}(D_x - D_y) \tag{2}$$

The rhombicity of **D** is given by the ratio $\lambda = E/D$. The principal axes are chosen such that $|D_z| > |D_y| > |D_x|$ and thus $0 < \lambda < 1/3$.

Table 1
Spin Hamiltonian parameters that best reproduce the experimental spectra. The strains are quantified by the FWHM of the Gaussian distribution in the *D*- and *E*-values. Errors are estimated from the sensitivity of the calculated spectrum to a variation in a parameter: ±0.5 GHz for the zero-field-splitting parameters, ±0.001 for the *g*-values and ±0.5 GHz for the strains. The spectra of rubredoxin are relatively insensitive to a change in g_x. The error in this parameter is estimated to be ±0.005. The error in the measured magnetic field values was estimated to be 2 mT at 10 T and gives a negligible contribution.

	D (GHz)	E (GHz)	λ	g_x	g_y	g_z	D-strain (GHz)	E-strain (GHz)
Fe(III)–EDTA	−23.3	−6.3	0.27	2.004	2.004	2.005	4.3	1.7
D. gigas Rd	47.5	12.5	0.26	2.02	2.021	2.014	9.0	2.5
P. furiosus Rd	49.5	13.0	0.26	2.02	2.021	2.014	9.0	2.5
M. elsdenii Rd	48.5	13.0	0.27	2.02	2.021	2.014	9.0	2.5

In the weak-field limit ($\widetilde{\mathbf{S}}\mathbf{D}\mathbf{S} \gg \mu_B\widetilde{\mathbf{S}}\mathbf{g}\mathbf{B}$) the effective $S = 1/2$ picture, in which the effect of the zero-field splitting can be incorporated in an effective *g*-tensor, is applicable. This is the case when rubredoxin is studied at X-band. The absolute value and sign of *D* can be determined only indirectly from the temperature dependence of the spectra and the effective *g*-values at which resonances are observed [38].

In the high-field limit ($\widetilde{\mathbf{S}}\mathbf{D}\mathbf{S} \ll \mu_B\widetilde{\mathbf{S}}\mathbf{g}\mathbf{B}$) the frozen solution spectrum shows the transitions associated with the principal axes of the *g*-tensor, because the energy levels vary linearly with the field strength. At low temperature the large polarization effect greatly simplifies the spectra and the sign of *D* can be determined from the spectra directly [28]. Transitions arising from one principal direction are separated in field by:

$$\Delta B = \frac{3D_i}{\mu_B g_i} \tag{3}$$

where *i* is *x*, *y* or *z*. The case of Fe(III)–EDTA at 275 GHz is near the high-field limit. Resonances are observed at 6.6 T, 8.2 T and 9.85 T. These resonances are roughly 1.6 T apart, which gives an absolute value of about 15 GHz for the largest principal value of **D**, D_z. Since these resonances are observed below $g = 2$, the sign of D_z is negative. A resonance is observed at 11.3 T, which is 1.45 T above 9.85 T. From this we estimate $D_y \approx 14$ GHz, which gives $D \approx -22.5$ GHz and $E \approx -6.5$ GHz.

In the intermediate region the ZFS-term and the Zeeman term are similar in size. This is the situation of rubredoxin at 275 GHz. As can be seen in Fig. 5 this gives rise to complex spectra. The way to extract the spin Hamiltonian parameters from the observed spectra is by comparison with spectra that were calculated by numerical diagonalization of the spin Hamiltonian. For this we used EasySpin [39]. We assume that the *D*- and *g*-tensor are collinear.

The spin Hamiltonian parameters that were found to fit the experimental spectra of the different types of rubredoxin best are shown in Table 1. The resonances below 4 T are due to forbidden transitions. The shape of the resonance around 4 T strongly depends on λ. The positions of the 6.8 T, 10.1 T and 11.3 T resonances are determined by the values of *E* and *D*. The position of the resonance at 8.7 T is influenced by both *D* and g_x. The values of g_y and g_z are determined by the positions of the 9.5 T and 9.7 T resonances respectively.

Also the Fe(III)–EDTA spectra were compared with spectra calculated with EasySpin and the parameters with which these spectra were best reproduced are summarized in Table 1. The value of D_z is determined by the position of the resonance around 6.6 T. The value of g_z must be slightly higher than g_x and g_y to reproduce the shape of the spectrum just below 9.8 T.

The resonances of the Fe(III)–EDTA are broader when they are further away from $g = 2$. Transitions between energy levels that have the larger $|m|$ are broader, which points to the presence of *D*- and *E*-strain. In fact the shape of the observed spectra of both Fe(III)–EDTA and rubredoxin could only be reproduced by taking into account *D*- and *E*-strain in the EasySpin calculations (see Table 1).[3] No additional isotropic line-broadening was taken into account.

5. Discussion

The modifications to our spectrometer have made it possible to acquire high-quality cw EPR spectra at 275 GHz on 25 nl of a 1 mM frozen solution of the high-spin Fe^{3+} model complex Fe(III)–EDTA. We have also acquired high-quality spectra of 10 mM frozen solutions of the high-spin Fe^{3+} protein rubredoxin. The signal-to-noise ratio of these spectra is such that a lower protein concentration could have been used. The sensitivity and baseline stability of our spectrometer are high enough to resolve resonances that have a width of 1 T in spectra that are acquired at low temperature, range over 12 T and require several hours to record. The quality of the spectra allows accurate determination of the parameters of the spin Hamiltonian by comparison to spectra that were calculated from numerical diagonalization of the spin Hamiltonian while taking into account line broadening due to *D*- and *E*-strain.

The sensitivity that can be obtained with a particular spectrometer for a particular system in practice depends on the width of the resonance that has to be recorded, the modulation amplitude that can be generated and the microwave power that can be applied. The spectrum shown in Fig. 2 from which we determined the absolute sensitivity of our spectrometer to be $8{\cdot}10^8$ spins/mT/$\sqrt{Hz}$ was acquired at maximum power and with a modulation amplitude that was optimal with respect to the line width.

The absence of slits and the complete closure of the cw cavity for microwaves by means of the choke joints assures that the quality factor of the cw cavity is higher than that of the general purpose cavity [14]. To estimate this increase we have determined the length of a $\pi/2$-pulse for a single crystal of gamma-ray irradiated lithium fluoride ($S = 1/2$). At room temperature this is 160 ns for the cw cavity and approximately 340 ns for the general purpose cavity. This corresponds to a twofold increase in the B_1-field in the cavity and an expected fourfold increase in signal intensity. Continuous-wave spectra recorded on TEMPO in toluene show that the absolute sensitivity at room temperature is approximately five times higher for the cw cavity. The additional increase is mainly due to improved coupling of the microwaves into the cavity.

The absolute sensitivity of our spectrometer is on the high end of the range of sensitivities achieved with other HF EPR spectrometers [4–13,16]. In order to study high-spin metalloproteins by cw HF EPR, high sensitivity is a primary condition that must be fulfilled. Signal stability is as important, particularly for

[3] In the online documentation on EasySpin the author notes that the effect of strains on the spectra are calculated using an approximation, which is only applicable as long as the strain distribution width is much smaller than the parameter itself. In our situation this is not immediately clear. However spectra that were calculated by running a loop over a distribution of spin Hamiltonian parameters matched almost exactly with the spectra that were calculated in the (much less time consuming) EasySpin approximation. The approximation is thus valid.

metalloproteins that show a large zero-field splitting. Hence, during low temperature experiments temperature and pressure in the cryostat must be controlled precisely. And microphonics must be minimized. The construction of a cavity that is completely closed for microwaves and the specific construction of the modulation coil have been instrumental in accomplishing this.

The quality of the spectra that we recorded on a 25 nl sample of 1 mM Fe(III)–EDTA is comparable to the quality accomplished by other authors at 285 and 244 GHz at concentrations that were higher by a factor of 60 or more [16,26,27]. The quality of the spectra acquired at 230 GHz as reported in [28] at 10 mM is slightly better than ours.

The chemistry of Fe(III)–EDTA in solution is very complex, which makes it difficult to compare spin Hamiltonian parameters found in various experiments. The coordination of the iron ion in EDTA is pH dependent as is its EPR spectrum [40,41]. A study of Fe(III)–EDTA in the form of a crystalline powder of Co(III)–EDTA with impurities of ferric ions, ratio Co:Fe = 50:1, at X-band and Q-band gave $|D|$ = 24.9 GHz and E/D = 0.31 [42]. The X-band spectrum from this study is reproduced with the parameters that were found from our experiments, except for the *D*- and *E*-strain which must be set to zero and instead an isotropic line broadening of 3 mT must be introduced. Our spin Hamiltonian parameters resemble closely the values reported in Ref. [28]. In this study no *D*- and *E*-strain were taken into account.

Rubredoxin from several organisms has been studied at the standard EPR frequency of 9 GHz [29,38,43–45]. The *D*-values are around 50 GHz and the rhombicity parameter λ is around 0.26. This is in line with our results. The natural variety in the amino-acid sequences of rubredoxins from different organisms results in small variations in the geometrical structure of the active site of the protein [31,34]. This will lead to subtle variations in the electronic structure of the active site, which can very well be studied by HF EPR [46]. Fig. 6 shows that at 275 GHz a change of 1 GHz in one of the zero-field-splitting parameters is obvious from the spectra. The quality of our spectra is such that we are able to determine the zero-field-splitting parameters with an accuracy of 0.5 GHz by comparison to spectra calculated from numerical diagonalization of a spin Hamiltonian.

The *D*- and *E*-strain that had to be included in the simulations to reproduce the experimental spectra is comparable in size for the model complex and the protein. A considerable active-site heterogeneity is common for proteins, but not for Fe(III)–EDTA. Heterogeneity in the coordination of the iron ion could be an explanation [47].

Börger et al. interpreted the complicated frozen solution spectrum of rubredoxin at X-band by including E/D-strain into their simulations [45]. From X-band spectra the strain in *D* and *E* can not be determined independently. They found a Gaussian distribution of E/D with a width of $\sigma_{E/D}$ = 0.03. If we take the square root of the sum of the squares of our relative *D*- and *E*-strain, we find a relative E/D-strain of 11%. On average the value of E/D found for rubredoxin is 0.26, which gives a value of 0.03 for $\sigma_{E/D}$.

The precise positions of the resonances around $g = 2$ made it necessary for both Fe(III)–EDTA and rubredoxin to include a small *g*-anisotropy in the simulations. The high magnetic field at which the spectra were recorded made it possible to determine reliable *g*-values directly. These *g*-values are clearly different from the *g*-values that were determined earlier, indirectly, from X-band spectra [45].

6. Conclusion

Our studies of high-spin Fe^{3+} systems show that we are able to acquire high-quality HF cw EPR spectra of frozen solutions of small amounts of modest size metalloproteins. The quality of the spectra is high enough to observe *g*-anisotropy and to determine the zero-field-splitting parameters with an accuracy of 0.5 GHz.

The success of our approach results partially from the enhanced absolute sensitivity that can be reached using a single-mode cavity, which was specifically constructed to be used for cw HF EPR. At least as important is the achieved signal stability.

Acknowledgment

The research was supported with financial aid by The Netherlands Organization for Scientific Research (NWO), Department of Chemical Sciences (CW).

Appendix A. Supplementary material

Supplementary data associated with this article can be found, in the online version, at doi:10.1016/j.jmr.2011.03.009.

References

[1] O.Y. Grinberg, A.A. Dubinskii, V.F. Shuvalov, L.G. Oranskii, V.I. Kurochkin, Y.S. Lebedev, Submillimeter EPR spectroscopy of free-radical, Dokl. Akad. Nauk. 230 (1976) 884–887.
[2] A.A. Galkin, O.Y. Grinberg, A.A. Dubinskii, N.N. Kabdin, V.N. Krymov, V.I. Kurochkin, Y.S. Lebedev, L.G. Oranskii, V.F. Shuvalov, EPR spectrometer in 2-mm range for chemical research, Instrum. Exp. Tech. 20 (1977) 1229–1233.
[3] O.Y. Grinberg, A.A. Dubinskii, Biological Magnetic Resonance 22 – Very High Frequency (VHF) ESR/EPR, Kluwer Academic/Plenum Publishers, 2004, pp. 1–18.
[4] W.B. Lynch, K.A. Earle, J.H. Freed, 1-mm wave ESR spectrometer, Rev. Sci. Instrum. 59 (1988) 1345–1351.
[5] K.A. Earle, D.S. Tipikin, J.H. Freed, Far-infrared electron-paramagnetic-resonance spectrometer utilizing a quasi-optical reflection bridge, Rev. Sci. Instrum. 67 (1996) 2502–2513.
[6] F. Muller, M. Hopkins, N. Coron, M. Grynberg, L.C. Brunel, G. Martinez, A high magnetic field EPR spectrometer, Rev. Sci. Instrum. 60 (1989) 3681–3684.
[7] A.L. Barra, L.C. Brunel, J.B. Robert, EPR spectroscopy at very high field, Chem. Phys. Lett. 165 (1990) 107–109.
[8] P. Neugebauer, A.-L. Barra, New cavity design for broad-band quasi-optical HF-EPR spectroscopy, Appl. Magn. Reson. 37 (2010) 833–843.
[9] G.M. Smith, J.C.G. Lesurf, R.H. Mitchell, P.C. Riedi, Quasi-optical cw mm-wave electron spin resonance spectrometer, Rev. Sci. Instrum. 69 (1998) 3924–3937.
[10] M.R. Fuchs, T.F. Prisner, K. Mobius, A high-field/high-frequency heterodyne induction-mode electron paramagnetic resonance spectrometer operating at 360 GHz, Rev. Sci. Instrum. 70 (1999) 3681–3683.
[11] M. Rohrer, J. Krzystek, V. Williams, L.-C. Brunel, Fabry-Pérot resonator for high-field multi-frequency ESR at millimetre and submillimetre wavelengths, Meas. Sci. Technol. 10 (1999) 275–284.
[12] A.K. Hassan, L.A. Pardi, J. Krzystek, A. Sienkiewicz, P. Goy, M. Rohrer, L.-C. Brunel, Ultrawide band multifrequency high-field EMR technique: a methodology for increasing spectroscopic information, J. Magn. Reson. 142 (2000) 300–312.
[13] M. Rohrer, O. Brügmann, B. Kinzer, T.F. Prisner, High-field/high-frequency EPR spectrometer operating impulsed and continuous-wave mode at 180 GHz, Appl. Magn. Reson. 21 (2001) 257–274.
[14] H. Blok, J.A.J.M. Disselhorst, S.B. Orlinskii, J. Schmidt, A continuous-wave and pulsed electron spin resonance spectrometer operating at 275 GHz, J. Magn. Reson. 166 (2004) 92–99.
[15] H. Blok, J.A.J.M. Disselhorst, H. van der Meer, S.B. Orlinskii, J. Schmidt, A continuous-wave and pulsed electron spin resonance spectrometer operating at 275 GHz, J. Magn. Reson. 173 (2005) 49–53.
[16] E. Reijerse, P.P. Schmidt, G. Klihm, W. Lubitz, A cw and pulse EPR spectrometer operating at 122 and 244 GHz using a quasi-optical bridge and a cryogen-free 12 T superconducting magnet, Appl. Magn. Reson. 31 (2007) 611–626.
[17] K. Mobius, A. Savitsky, High-Field EPR Spectroscopy on Proteins and their Model Systems – Characterization of Transient Paramagnetic States, The Royal Society of Chemistry, Cambridge, 2009, pp. 124–194.
[18] E. Reijerse, High-frequency EPR instrumentation, Appl. Magn. Reson. 37 (2010) 795–818.
[19] G. Feher, Sensitivity considerations in microwave paramagnetic resonance absorption techniques, Bell Syst. Tech. J. (1957) 449–484.
[20] C.P. Poole Jr., Electron Spin Resonance – A Comprehensive Treatise on Experimental Techniques, John Wiley & Sons, 1983.
[21] G.R. Eaton, S.S. Eaton, G.A. Rinard, Spatially Resolved Magnetic Resonance, Wiley-VCH, 1998, pp. 65–74.
[22] G.A. Rinard, R.W. Quine, J.R. Harbridge, R. Son, G.R. Eaton, S.S. Eaton, Frequency dependence of EPR signal-to-noise, J. Magn. Reson. 140 (1999) 218–227.
[23] J.S. Hyde, Foundations of Modern EPR, World Scientific, 1997, pp. 695–716.

[24] D.E. Budil, K.A. Earle, Biological Magnetic Resonance 22 – Very High Frequency (VHF) ESR/EPR, Kluwer Academic/Plenum Publishers, 2004, pp. 353-399.
[25] D.T. Teaney, M.P. Klein, A.M. Portis, Microwave superheterodyne induction spectrometer, Rev. Sci. Instrum. 32 (1961) 721–729.
[26] K.K. Andersson, A.-L. Barra, The use of high - field/frequency EPR in studies of radical and metal sites in proteins and small inorganic models, Spectrochim. Acta, Part A 58 (2002) 1101–1112.
[27] K.K. Andersson, P.P. Schmidt, B. Katterle, K.R. Strand, A.E. Palmer, S.-K. Lee, E.I. Solomon, A. Gräslund, A.-L. Barra, Examples of high-frequency EPR studies in bioinorganic chemistry, J. Biol. Inorg. Chem. 8 (2003) 235–247.
[28] A.-L. Barra, A. Gräslund, K.K. Andersson, Biological Magnetic Resonance 22 – Very High Frequency (VHF) ESR/EPR, Kluwer Academic/Plenum Publishers, 2008, pp. 145–163.
[29] J. Meyer, J.-M. Moulis, Handbook of Metalloproteins, Wiley & Sons, 2001, pp. 505–517.
[30] M. Frey, L. Sieker, F. Payan, R. Haser, M. Bruschi, G. Pepe, J. LeGall, Rubredoxin from *Desulfovibrio gigas* – a molecular model of the oxidized form at 1.4 Å resolution, J. Mol. Biol. 197 (1987) 525–541.
[31] C.-J. Chen, Y.-H. Lin, Y.-C. Huang, M.-Y. Liu, Crystal structure of rubredoxin from *Desulfovibrio gigas* to ultra-high 0.68 Å resolution, Biochem. Biophys. Res. Commun. 349 (2006) 79–90.
[32] R.M. Almeida, S.R. Pauleta, I. Moura, J.J.G. Moura, Rubredoxin as a paramagnetic relaxation-inducing probe, J. Inorg. Biochem. 103 (2009).
[33] M.W. Day, B.T. Hsu, L. Joshua-Tor, J.-B. Park, Z.H. Zhou, M.W.W. Adams, D.C. Rees, X-ray crystal structures of the oxidized and reduced of the rubredoxin the marine hyperthermophilic archaebacterium *Pyrococcus furiosus*, Protein Sci. 1 (1992) 1494–1507.
[34] R. Bau, D.C. Rees, D.M. Kurtz, R.A. Scott, H. Huang, M.W.W. Adams, M.K. Eidsness, Crystal structure of rubredoxin from *Pyrococcus furiosus* at 0.95 Å resolution, and the structures of n-terminal methionine and formylmethionine variants of Pf Rd. contributions of *N*-terminal interactions to thermostability, J. Biol. Inorg. Chem. 3 (1998) 484–493.
[35] P.R. Blake, J.B. Park, F.O. Bryant, S. Aono, J.K. Magnuson, E. Eccleston, J.B. Howard, M.F. Summers, M.W.W. Adams, Determinants of protein hyperthermostability: purification and amino acid sequence of rubredoxin from the hyperthermophilic archaebacterium *Pyrococcus furiosus* and secondary structure of the zinc adduct by NMR, Biochemistry 30 (1991) 10885–10891.
[36] S.G. Mayhew, J.L. Peel, Rubredoxin from *Peptostreptococcus elsdenii*, Biochem. J. 100 (1966) 80.
[37] L.A. Pardi, J. Krzystek, J. Telser, L.-C. Brunel, Multi-frequency EPR spectra of molecular oxygen in solid air, J. Magn. Reson. 146 (2000) 375–378.
[38] W.E. Blumberg, J. Peisach, The measurement of zero field splitting and the determination of ligand composition in mononuclear nonheme iron proteins, Ann. NY Acad. Sci. 222 (1973) 539–560.
[39] S. Stoll, A. Schweiger, Easyspin, a comprehensive software package for spectral simulation and analysis in EPR, J. Magn. Reson. 178 (2006) 42–55.
[40] C. Bull, G.J. McClune, J.A. Fee, The mechanism of Fe-edta catalyzed superoxide dismutation, J. Am. Chem. Soc. 105 (1983) 5290–5300.
[41] S. Fujii, H. Ohya-Nishiguchi, N. Hirota, EPR evidence of intermediate peroxo complexes formed in a SOD model system, Inorg. Chim. Acta 175 (1990) 27–30.
[42] R. Aasa, Powder line shapes in the electron paramagnetic resonance spectra of high-spin ferric complexes, J. Chem. Phys. 52 (1970).
[43] J. Peisach, W.E. Blumberg, E.T. Lode, M.J. Coon, An analysis of the electron paramagnetic resonance spectrum of *Pseudomonas oleovorans* rubredoxin, J. Biol. Chem. 246 (1971) 5877–5881.
[44] I. Moura, A.V. Xavier, R. Cammack, M. Bruschi, J.L. Gall, A comparative spectroscopic study of two non-haem iron proteins lacking labile sulphur from *Desulfovibrio gigas*, Biochim. Biophys. Acta 533 (1978) 156–162.
[45] B. Börger, D. Suter, Magnetic and optical anisotropy of *Clostridium pasteurianum* rubredoxin from optically detected electron paramagnetic resonance, J. Phys. Chem. 115 (2001) 9821–9826.
[46] A. Barra, A. Hassan, A. Janoschka, C.L. Schmidt, V. Schünemann, Broad-band quasi-optical HF-EPR spectroscopy: application to the study of the ferrous iron center from a rubredoxin mutant, Appl. Magn. Reson. 30 (2006) 385–397.
[47] R. Meier, F.W. Heinemann, Structures of the spontaneously resolved six-coordinate potassium chloro-(ethylenediaminetriacetato acetic acid) iron(iii) monohydrate and the seven-coordinate potassium (ethylenediaminetetracetato) iron(iii) sesquihydrate, Inorg. Chim. Acta 337 (2002) 317–327.